

1 **Simulating the transportation and dispersal of volcanic**
2 **ash cloud with initial condition created by 3D plume**
3 **model**

4 **Key Points:**

- 5 • Creating initial conditions for volcanic ash transport and dispersal models based
6 on 3D plume model output eliminates need for assumptions or inversion regard-
7 ing initial ash particle distribution with height, and improves prediction capabil-
8 ity.
- 9 • Initial particle distribution in vertical direction has greater impact on transport
10 of ash clouds than does horizontal distribution.
- 11 • Ash particles involved in long-range transport are initially concentrated in the um-
12 brella cloud of large eruptions.

13 **Abstract**

14 VATDs (volcanic ash transportation and dispersion) model atmospheric transport of ash
 15 starting from a source originating at the volcano represented by concentrations of ash
 16 with height. Most VATD models use a line source of some prescribed shape calibrated
 17 against an empirical expression for the height-mass eruption rate (MER) relation. Such
 18 empirical vertical ash distributions are often inadequate representations of actual ver-
 19 tical ash distributions, which usually vary from case to case and have complex depen-
 20 dencies on eruption source parameters and atmospheric conditions. We present here for
 21 the first time the use of 3D (three-dimensional) plume models to represent ash cloud source
 22 without any assumption regarding plume geometry. By eliminating assumed behavior
 23 associated with the semiempirical plume geometry, the predictive skill of VATD simu-
 24 lations are greatly improved. To date no VATD simulation adopt initial condition cre-
 25 ated from first principles based 3D plume simulation. We use our recently developed vol-
 26 canic plume model based on a 3D Lagrangian method [Cao et al, Geophysical Model Dev.,
 27 2018] and couple the output to a standard Lagrangian VATD model and apply to his-
 28 torical eruptions to illustrate the effectiveness of this approach. The importance of the
 29 source model is shown in sensitivity analyses which prove that volcanic ash transpor-
 30 tation simulation is much more sensitive to the source geometry than all other input pa-
 31 rameters. Further investigation also reveals that initial particle distribution in vertical
 32 direction has more impact on transportation of ash clouds than horizontal distribution.
 33 Comparison also indicates that ash particles are concentrated along intrusion height of
 34 umbrella cloud that is much lower than the plume top, which is just momentum over-
 35 shoot.

36 **1 Introduction**

37 **1.1 Volcanic Ash Transportation Forecast**

38 The fine-grain fraction of tephra (volcanic ash) can be widely dispersed, and can
 39 lead to a degradation of air quality and pose threats to aviation (Tupper et al., 2007).
 40 Identification of volcanic ash helps schedule flights to avoid areas where ash is present.
 41 Numerical estimation of ash distribution using known and forecast wind fields is neces-
 42 sary if we are to accurately predict ash cloud evolution. Numerous VATD (volcanic ash
 43 transportation and dispersion) models have been developed by both civil and military
 44 aviation or meteorological agencies to provide forecasts of ash cloud motion (Witham
 45 et al., 2007). New techniques have been integrated with VATDs to satisfy increasing de-
 46 mands for more outputs, model accuracy and forecast reliability. This contribution ex-
 47 plores a method for creating initial conditions for VATD simulations, which promises to
 48 improve prediction capability and accuracy.

49 ?Stohl et al. (2011) showed that initial source conditions have significant effects on
 50 simulation of volcanic ash transportation. Traditional VATD simulation requires key global
 51 descriptors of the volcanic plumes, especially plume height, grain size, eruption duration
 52 and mass loading, or alternatively, a mass eruption rate (MER). No matter how these
 53 global descriptors are obtained, they are used to furnish the initial conditions for VATDs
 54 in the form of a line-source term of a spatio-temporal distribution of particle mass. It
 55 is a common practice to pick values for these global descriptors using an empirical ex-
 56 pression for the height-MER relation. The empirical expression is written as a function
 57 of several parameters, including the key global descriptors. The values for the descrip-
 58 tors can also be found by parameter calibration (e.g. ??Stohl et al., 2011; Zidikheri et
 59 al., 2017). 1D plume models serve as an alternative option to provide values. For exam-
 60 ple, ? and “stefanescu2014temporal” (n.d.) used the 1D model puffin (Bursik, 2001) to
 61 generate estimates of mass eruption rate and grain size. In some cases, an extra step is
 62 adopted to spread ash particles from the line source horizontally, resulting in an initial
 63 ash cloud in 3D space. The horizontal spreading depends on an empirical expression. For

example, the VATD model Puff spreads particles from the line source uniformly in the horizontal direction within a given radius using an empirical expression in puffin. Considering the complexities of volcanic eruptions, the actual ash distribution in initial ash clouds should vary from case to case and with time, making it difficult to find one general expression that is suitable for all cases. It is useful therefore to investigate alternative ways for creating initial ash clouds without assumptions regarding plume geometry or numerical inversion. This provides the major motivation of this paper.

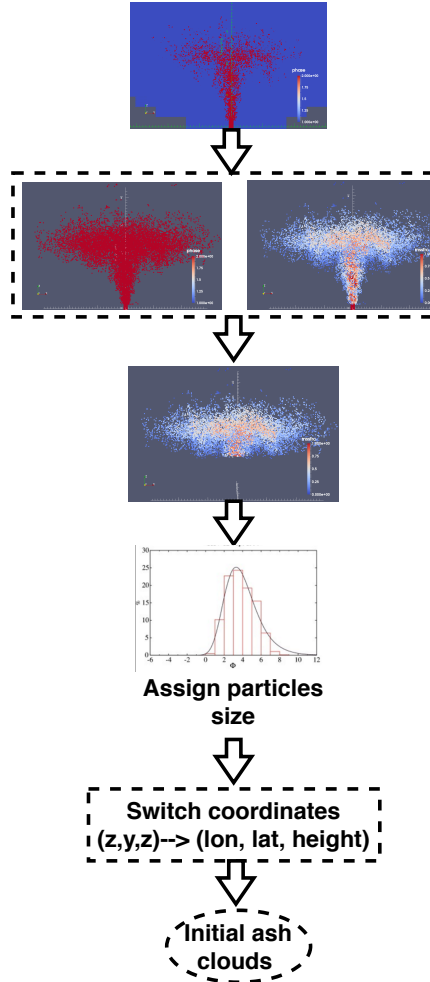
1.2 Numerical Tools

VATD models can be categorized into Lagrangian particle tracking and Eulerian advection-diffusion types. Among several available particle tracking models (e.g. Walko et al., 1995; Searcy et al., 1998; Damours, 1998; Draxler & Hess, 1998) and advection-diffusion models (e.g. Bonadonna & Houghton, 2005; Folch et al., 2009; Schwaiger et al., 2012), we adopt a particle tracking model, Puff (Tanaka, 1991; Searcy et al., 1998), as the VATD model. Puff can take 3D ash clouds as initial conditions, which makes it technically easier to couple with 3D plume models. Puff initializes a discrete number of tracers that represent a sample of the eruption cloud, and calculates transport, turbulent dispersion, and fallout for each representative tracer. A cylinder emanating vertically from the volcano summit to a specified maximum height is the standard approach to provide a simple model of the geometry of a typical ash column. Puff minimally requires horizontal wind field data. The “restart feature” of Puff makes it technically feasible to accommodate the hand-off between a plume simulation and the Puff simulation in terms of time and length scales.

Besides parameter calibration, 1D (one dimensional) plume models have been used to obtain global descriptors of volcanic plumes. 1D plume models (e.g. Woods, 1988; Buršík, 2001; Mastin, 2007; de'Michieli Vitturi et al., 2015; Folch et al., 2016; Pouget et al., 2016) solve the equations of motion in 1D using simplifying assumptions, and hence depend on estimation of certain parameters, especially those related to the entrainment of air, which is evaluated based on two coefficients: a coefficient due to turbulence in the rising buoyant jet, and one due to the crosswind field. Different 1D models adopt different entrainment coefficients based on a specific formulation or calibration against well-documented case studies. The feedback from plume to atmosphere is usually ignored in 1D models. While these 1D models generated well-matched results with 3D models for plumes that are much influence by wind, often called weak plumes, much greater variability is observed for strong plume scenarios (Costa et al., 2016). On the other hand, 3D numerical models for volcanic plumes based on first principles and having few parametrized coefficients (Oberhuber et al., 1998; Neri et al., 2003; Y. J. Suzuki et al., 2005; Cerninara, Esposti Ongaro, & Berselli, 2016; Cao et al., 2018) naturally create a 3D ash cloud, which could serve directly as an initial state of the volcanic material for VATDs. However, there is no VATD simulation using such 3D ash clouds as initial conditions. In this paper, we will carry out VATD simulations using an initial state for the ash cloud based on 3D plume simulations, generated with Plume-SPH (Cao et al., 2018). The implementation techniques described in this paper can be applied for any combination of VATD model and 3D plume model even though our investigation is based on a specific VATD model and plume model.

1.3 Pinatubo Eruption

The 1991 eruption of Pinatubo volcano is used as a case study. Pinatubo erupted between June 12 and 16, 1991, after weeks of precursory activity. The climactic phase started on June 15 at 0441 UTC and ended around 1341 UTC (?). The climactic phase generated voluminous pyroclastic flows, and sent Plinian and co-ignimbrite ash and gas columns to great altitudes (?). The evolution of the Pinatubo ash and SO_2 clouds was tracked using visible (?), ultraviolet (Total Ozone Mapping Spectrometer; TOMS) (?)



122 **Figure 1.** Work flow to create initial condition for Puff based on raw output of Plume-SPH.
123 Top: raw output of Plume-SPH. Blue particles are phase 1 (ambient air), red particles are phase
124 2 (erupted material). Second row: plume after removing SPH particles of phase 1. Left: colored
125 according to mass fraction of erupted material. Third row: volcanic plume above the “corner”
126 region after cutting off lower portion.

115 and infrared sensors, including the Advanced Very High-Resolution Radiometer (AVHRR)
116 (?). There are also sufficient observational data to estimate the eruption conditions for
117 the climactic phase of the eruption (Y. Suzuki & Koyaguchi, 2009). The availability of
118 calibrated eruption conditions and extensive observational data regarding ash clouds trans-
119 port make the Pinatubo eruption an ideal case study.

120 2 Setting up Simulations

121 2.1 Creation of Initial Ash Cloud

122 The steps to create an initial ash cloud based on the raw output of Plume-SPH are
123 shown in Fig. 1. The method proposed consists in generating the initial ash cloud di-
124 rectly from Plume-SPH, foregoing assumptions and estimates or inverse modeling regard-
125 ing ash injection height and timing thereof. We use Plume-SPH as an example, noting
126 that for other 3D plume models, the steps would be similar. Plume-SPH is a two-phase

model based on the Lagrangian smoothed-particle hydrodynamics (SPH) method, in which the computational domain is discretized by SPH particles. The current version, Plume-SPH 1.0 (Cao et al., 2018), uses two types of SPH particles: 1) particles of phase 1 to represent ambient air, and 2) particles of phase 2 to represent erupted material. The initial ash cloud is created from SPH particle of phase 2.

After reaching the maximum rise height and starting to spread horizontally, particles of phase 2 form an initial umbrella cloud (Fig. 2). The 3D plume simulation is considered complete once the umbrella cloud begins to form. Parcels that will be transported by the ambient wind are those above the “corner” region, where mean plume motion is horizontal rather than vertical.

Considering that SPH particles are only discretization points, each is assigned a grain size according to a given total grain size distribution (TGSD) (?), and a concentration according to the mass and volumetric eruption rate. The Plume-SPH discretization points are thus switched to Puff Lagrangian tracer particles having grain sizes and concentrations. The coordinates of these tracer particles, which are initially in the local Cartesian coordinate system of Plume-SPH, are converted into Puff’s global coordinate system, which is given in terms of (*longitude, latitude, height*). Puff takes the initial ash cloud, consisting of the collection of Lagrangian tracer particles with grain size and concentration, and propagates from time t to time $t+\Delta t$ via an advection/diffusion equation (Searcy et al., 1998).

$$\mathbf{R}_i(t + \Delta t) = \mathbf{R}_i(t) + \mathbf{W}(t)\Delta t + \mathbf{Z}(t)\Delta t + \mathbf{S}_i(t)\Delta t \quad (1)$$

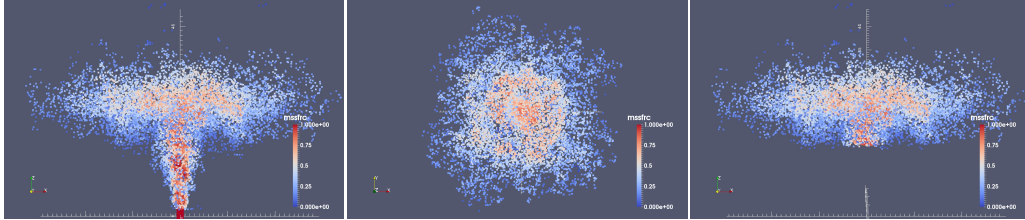
Here, $\mathbf{R}_i(t)$ is the position vector of the i^{th} Lagrangian tracer particle at time t , \mathbf{W} accounts for wind advection, \mathbf{Z} accounts for turbulent dispersion and \mathbf{S} is the terminal gravitational fallout velocity, which depends on tracer’s size.

To summarize, there are four steps to create an initial ash cloud from the raw output of Plume-SPH:

1. filter by SPH particle type to select SPH particles that represent erupted material (phase 2)
2. filter by a mean velocity threshold to select the upper part (above the “corner” region) dominated by horizontal transport
3. switch SPH discretization points to Lagrangian tracer particles, by assigning grain size to each particle
4. convert coordinates of the SPH Lagrangian tracers into the VATDs’ geographic coordinate system

The features of the volcanic plume and resulting initial ash cloud used in the case study are shown in Fig. 2. It is important to point out that since both Plume-SPH and Puff are based on the Lagrangian method, there is no extra step of conversion between an Eulerian grid and Lagrangian particles.

Table 1 compares three different methods for creating initial conditions for VATD simulation: 1) creating initial condition based on parameter calibration without any plume model (method 1), 2) creating initial condition based on output of 1D plume model (method 2), 3) extracting initial ash cloud from 3D plume simulation (method 3). The first method determines all global descriptors of volcanic plume based on calibration. Then create initial line source or ash cloud according to semiempirical plume shape expression. Both other two methods depend on plume models. However 3D plume models can generate initial ash cloud in 3D space while 1D plume models only obtain global descriptors of plume so still need semiempirical expression to create 3D initial ash cloud. In addition, the number of Lagrangian tracers is a free parameter when using semiempirical plume shape expressions while it purely depends on simulation when creating initial condition from 3D plume simulation results.



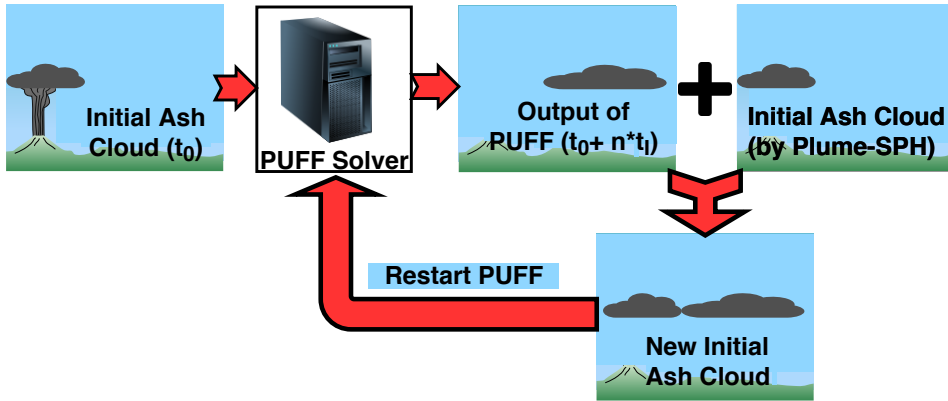
170 **Figure 2.** All particles in the pictures are of type phase 2 (phase 1 has been removed in step
 171 1) at 600s after eruption, at which time, the plume has already reached the maximum height
 172 and started spreading radially. Pictures from left to right are: front view of the whole plume,
 173 top view of the plume and front view of the initial ash cloud, which is essentially portion of the
 174 whole plume with elevation higher than a given threshold (in this picture is 15000m). Particles
 175 are colored according to mass fraction of erupted material. Red represents high mass fraction
 176 while blue represents low mass fraction.

189 **Table 1.** Three different methods for creating initial conditions (initial ash clouds) for Puff
 190 simulation

	No model	1D model	3D model
Maximum height	Calibration	Semiempirical	1st principle
Average height	Calibration	Conservation laws (1D)	1st principle
Vertical spread	Calibration	Semiempirical	1st principle
Column radius	Calibration	Conservation laws (1D)	1st principle
Plume shape	Semiempirical	Semiempirical	1st principle
Tracers number	Free parameter	Free Parameter	Based on simulation

191 2.2 Puff Restart

192 The plume and ash transport models are run at different time scales and length
 193 scales. The spatial and temporal resolutions of the plume simulations are much finer than
 194 those of the ash transport model. It takes tens of minutes (600s in this case) for the Pinatubo
 195 plume to reach a steady height. However the eruption persisted for a few hours (9 hours
 196 for the climactic phase of Pinatubo eruption), and it may be necessary to track ash trans-
 197 port for days following an eruption. At present, it is too expensive computationally to
 198 do 3D plume simulations of several hours in real time. In order to handle the difference
 199 in time scale, we mimic a continuing eruption with intermittent pulsed releasing of ash
 200 particles. Particularly, we restart Puff at an interval of 600s, i.e., the physical time of
 201 the plume simulation to reach steady height. At every Puff restart, we integrate the out-
 202 put of the last Puff simulation and Plume-SPH into a new ash cloud. This new ash cloud
 203 serves as a new initial condition with which to restart a Puff simulation. The interval
 204 of the pulsed releases is the simulation time of Plume-SPH, i.e., 600s in our case study.
 205 A sketch demonstrating the overall restart process is shown in Fig. (3). The total num-
 206 ber of Lagrangian tracer particles used in Puff thus equals the summed number of par-
 207 ticles in all releases. So the total number of tracer particles is no longer a user-selected
 208 parameter. ? proposed using more realistic time-dependent plume heights. We do not
 209 adopt that strategy here for simplicity, although the idea would be straightforward in
 210 execution.



211 **Figure 3.** Mimic successive eruption with intermittent pulsing releasing of ash particles. t_I is
212 the period of pulsing release. t_I equals to physical time of 3D plume simulation.

213 2.3 Sensitivity Analysis of Other Parameters

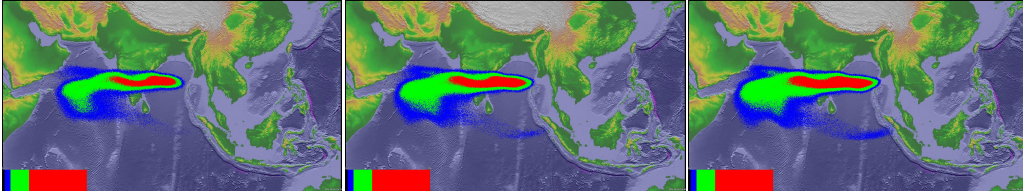
214 Besides the positions of particles in the initial ash cloud, other parameters for Puff
215 simulations are: horizontal diffusivity, vertical diffusivity, mean grain size, grain size stan-
216 dard deviation and total number of tracers. We present in this subsection systematic sen-
217 sitivity studies on these parameters. We also investigate the influence of eruption du-
218 ration. The sensitivity analyses will serve as the basis for identifying possible sources of
219 disparities between simulation and observation.

220 The sensitivity analyses illustrate that adjustment of other parameters produces
221 negligible visual differences in VATD simulation results. Using different vertical diffu-
222 sivities in range of $[100, 100000] m^2 s^{-1}$ and different horizontal diffusivities in range of
223 $[1, 20] m^2 s^{-1}$ produces visually negligible differences. The simulation eruption duration
224 should depend on the total observed duration or the duration of the climactic phase. We
225 conducted several simulations with eruption duration varying in range of $[5, 11] hours$ with
226 slight different starting time of climactic phase. Table 2 lists all these simulations. How-
227 ever, only tiny visible differences are observed among the simulated ash transportation.
228 The mean of grain size also has visually ignorable effects on long-term ash transporta-
229 tion according to our sensitivity tests varying the log mean (base 10) grain radius in a
230 range of $[-7.3, -3.5] m$. The standard deviation, when varying in range of $[0.1, 10]$, gen-
231 erate ignorable difference on long-term ash transportation as well. Similar conclusion on
232 parameter sensitivity is reported by ?Daniele et al. (e.g. 2009). Among these parame-
233 ters, the eruption duration and beginning time shows, even though tiny, the most ob-
234 vious influence on simulated ash distribution. In order to show such differences in an in-
235 tuitive way, Fig. 2 shows simulated ash distribution corresponding to 4.9 hours duration,
236 9 hours duration and 11 hours duration respectively. After 72 hours, relative to the sim-
237 ulation starting time, these three cases generate generally similar results, with high con-
238 centration ash covers almost the same region. The difference of lower concentration dis-
239 tribution is relatively more obvious. Ash cloud covers broadest area when eruption du-
240 ration is 11.1 hours. To summarize, all these parameters have either tiny or ignorable
241 affects on long-term ash distribution simulation.

247 The new methodology for generating initial ash cloud introduces another new pa-
248 rameter: elevation threshold. We also carry out sensitivity analysis on this parameter
249 by varying the elevation threshold from $1500 m$ (the height of the vent) to $25000 m$. The
250 simulated ash distributions show obviously visible differences. Such influence is especially
251 obvious when the elevation threshold is either very large or very small. However, vary-
252 ing the elevation threshold in the range of $[12000, 18000] m$ generates relatively small dif-

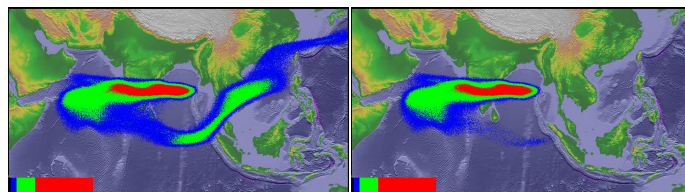
242 **Table 2.** The starting and ending time (UT) for simulating the climactic phase of Pinatubo
 243 eruption on June 15 1991. Observed plume height (?) at different time are also list in the table.

Eruption duration	4.9 hours	9 hours	10 hours	11.1 hours
Start time	0441	0441	0441	0334
Height at start time	37.5 km	37.5 km	37.5 km	24.5 km
End time	0934	1341	1441	1441
Height at end time	35 km	26.5 km	22.5	22.5 km



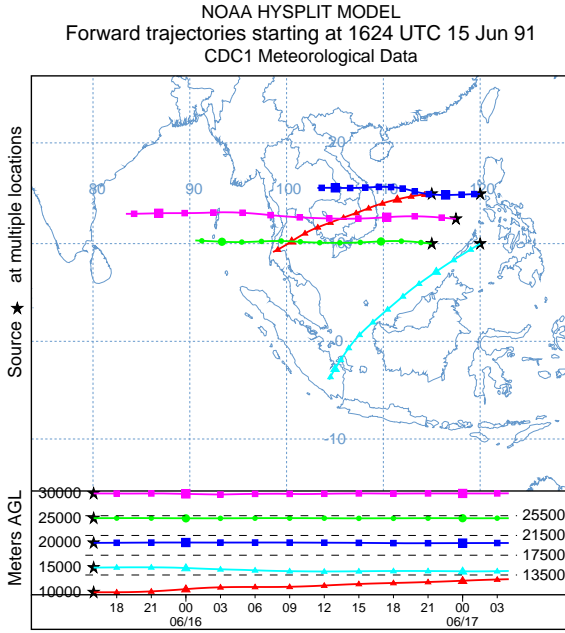
244 **Figure 4.** Simulated ash cloud distribution corresponding to eruption duration of 4.9 hours, 9
 245 hours and 11.1 hours (from left to right) respectively. Starting and ending time for each case is in
 246 Table 1. The contours are for ash distribution at 72 hours after eruption.

253 difference in ash transportation simulation results. Figure 5 compares the simulated ash
 254 distribution corresponding to elevation thresholds of 1500m and 15000m. Compared with
 255 ash distribution for threshold of 15000m, an extra long tail appears when using eleva-
 256 tion threshold of 1500m. Adopting smaller elevation thresholds essentially adds more trac-
 257 ers at lower elevation. As the wind at different elevations are different, these tracers at
 258 lower elevation would transpose to different directions. The forward trajectories, which
 259 starting at June 15 1624 UTC, indicates that the wind between evaluation 10000 m to
 260 15000 m blows from north-east to south-west while wind of higher evaluation blows from
 261 east to west.



262 **Figure 5.** Simulated ash distribution taking initial ash clouds obtained using different el-
 263 evation thresholds (1500m and 15000 m) from output of Plume-SPH. The contours are cor-
 264 responding to ash concentration at 72 hours after eruption. The starting and ending time are
 265 corresponding to 9 hours duration case in Table 2

268 The sensitivity analyses demonstrate that the initial condition for VATD sim-
 269 ulation has the most significant effect on simulated ash distribution while all other input
 270 parameters have either tiny or ignorable influence. The initial ash cloud generated based
 271 on semiempirical expression, which is a function of several parameters, might be signif-
 272 icantly disparate from realistic ash cloud. Such initial condition might greatly compro-
 273 mise the accuracy of VATDs simulation.



266 **Figure 6.** Trajectories of particles starting from different heights indicating the wind direction
267 of different evaluations.

274 We do not carry out any investigation with respect to wind field even though it is
275 another dominant factor in VATD simulation. In the case study, we use global *NOAA/OAR/ESRL6-*
276 *h*, 2.0° reanalysis wind fields data (???).

277 3 Comparison and Discussion

278 Transportation of volcanic ash resulted from Pinatubo eruption on June 15th 1991
279 is simulated using two different initial conditions. The initial condition is created in tra-
280 ditional way according to key global descriptors and semiempirical plume shape expres-
281 sion. The second initial condition is created by the new method proposed in this paper.
282 Simulated ash transportation results are compared against observation.

284 To create initial condition using the new method described in this paper, the plume
285 raising up process is simulated first by Plume-SPH. The eruption parameters, material
286 properties and atmosphere for the strong plume no wind case in a comparison study on
287 eruptive column models (Costa et al., 2016) are adopted. Eruption conditions and ma-
288 terial properties are listed in Table 3. Note that the density of erupted material at the
289 vent and radius of the vent can be computed from the given parameters. The eruption

283

Table 3. List of eruption condition and material properties for plume simulation

Parameters	Units	Plume
Vent velocity	$m \cdot s^{-1}$	275
Vent gas mass fraction		0.05
Vent Temperature	K	1053
Vent height	m	1500
Mass discharge rate	$kg \cdot s^{-1}$	1.5×10^9
Specific heat of gas at constant volume	$J \cdot kg^{-1} \cdot K^{-1}$	717
Specific heat of air at constant volume	$J \cdot kg^{-1} \cdot K^{-1}$	1340
Specific heat of solid	$J \cdot kg^{-1} \cdot K^{-1}$	1100
Specific heat of gas at constant pressure	$J \cdot kg^{-1} \cdot K^{-1}$	1000
Specific heat of air at constant pressure	$J \cdot kg^{-1} \cdot K^{-1}$	1810
Density of air at vent height	$kg \cdot m^{-3}$	1.104
Pressure at vent height	Pa	84363.4

290
291
292
293
294
295

pressure is assumed to be the same as pressure of ambient at the vent and hence is not given in the table. The vertical profiles of atmospheric properties were obtained based on the reanalysis data from ECMWF (European Centre for Medium-Range Weather Forecasts) for the period corresponding to the climactic phase of the Pinatubo eruption. The initial ash cloud is obtained by processing the raw output of Plume-SPH following steps described in Sec. 2.

296
297
298
299
300
301
302

Another set of initial condition is created based on observed top height (40km) and several other parameters assigned semiempirically (?). These parameters, namely, the global descriptors of volcanic plume, are used as parameters of semiempirical expression to get ash cloud in 3D space. See details in Table 4. Except for initial condition, the simulation parameters that control VATD simulation are the same for both simulations. As has been shown in sensitivity analyses section, these parameters have less influence on simulation results than initial condition.

307

3.1 “Plume-SPH + Puff” and “Semiempirical Initial Cloud + Puff”

308
309

The simulation results using different initial conditions are compared with TOMS images and AVHRR BTD ash cloud map in Fig. 7.

310
311
312
313
314
315
316
317
318
319
320
321
322
323
324
325
326
327
328
329
330
331
332
333
334
335

The differences between simulated ash transportation by “Semiempirical initial cloud +Puff” and “Plume-SPH+Puff” are obvious. The simulated ash concentration based on initial condition created from Plume-SPH is much closer to observation than that based on semiempirical plume shape expression. Around 23 hours and 31 hours after the beginning of the climactic phase, “Plume-SPH + Puff” simulation generates ash images that generally close to observational image, especially the location where high concentration ash presents. However, these ash at near west to Pinatubo mountain observed in satellite images does not show up in “Plume-SPH + Puff” simulation results. This disparity is very possible due to the fact that the Mountain Pinatubo continued erupting after climactic phase while our simulation only simulates the climactic phase. The ash released after climactic phase is not accounted in our simulation results. The “Semiempirical initial cloud + Puff” simulation, however, forecasts an ash distribution faster and narrower than observation. The location, where the high concentration ash presents, locates to the far northwest of observed ash. Around 55 hours after the beginning of the climactic phase, the disparity between observation and simulation becomes more obvious. Ash distribution of “Semiempirical initial cloud + Puff” simulation locates far west to the observed ash. The high concentration area of “Plume-SPH + Puff” simulation,

303 **Table 4.** Parameters used in VATD simulation of the climactic phase of Pinatubo eruption on
 304 June 15 1991. The first six parameters are used by semiempirical expression to create initial ash
 305 cloud. When create initial condition based on Plume-SPH model, these parameters are extracted
 306 from output of Plume-SPH model.

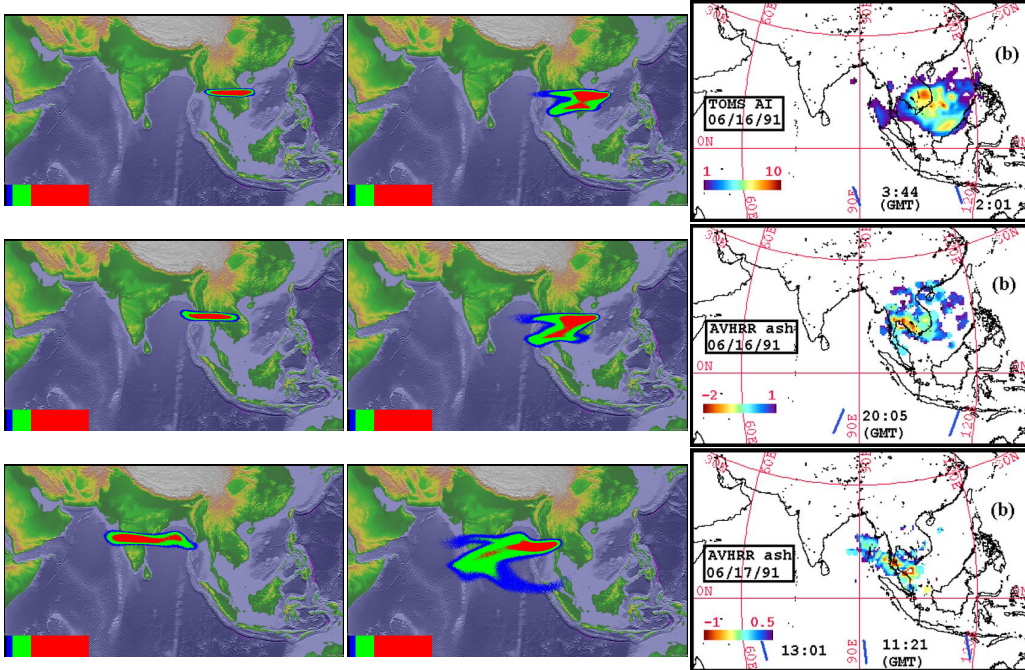
Parameters	Unit	Semiempirical	Plume-SPH
Maximum Height (H_{max})	m	40000	41800
Horizontal Spread (R_{max})	km	103.808	-
Vertical Spread (H_{width})	km	6.662	-
Plume Shape	-	Poisson	-
Total Ash Particles	-	1768500	1768500
Elevation Threshold	m	-	15000
Horizontal Diffusivity	m^2/s	10000	10000
Vertical Diffusivity	m^2/s	10	10
Grain Size Distribution	-	Gaussian	Gaussian
Mean of Grain Size (Radius)	mm	3.5×10^{-2}	3.5×10^{-2}
Standard Deviation of Grain Size	-	1.0	1.0
Start Time	UT	0441	0441
End time	UT	1341	1341
Simulation Duration	hour	72	72

336 even though closer to observation than that of “Semiempirical initial cloud +Puff”, is
 337 still faster than observation.

338 At the stage of ash transportation simulation, except for the initial condition, both
 339 simulations adopt the same parameters and wind field data. That is to say, the only dif-
 340 ference between these two simulations is the initial condition. Recall the initial condi-
 341 tion has most significant influence on ash transportation simulation. It is very possible
 342 that the big difference between simulation results by “Plume-SPH+Puff” and “Semiem-
 343 pirical initial cloud +Puff” is attribute to the initial condition. The ash transportation
 344 simulation based on 3D plume simulation results is much more accurate than that based
 345 on semiempirical initial cloud.

346 3.2 Discussion Regarding Maximum Height (H_{max})

347 In this section, we mainly discuss the vertical distribution of ash particles in ini-
 348 tial ash cloud. The majority of volcanic ash particles usually present a lower elevation
 349 than maximum height. For instance, ?? reported the maximum Pinatubo plume height
 350 as high as around 39km while the cloud heights were estimated at 20 ~ 25km, ? re-
 351 port the maximum plume height could be > 35km and the plume heights are 23 ~ 28km
 352 after 15 ~ 16 hours. The neutral buoyant regions of the Pinatubo aerosol estimated
 353 by different measurements are: 17 ~ 26km (lidar) by ?, 20 ~ 23km (balloon) by ?,
 354 17 ~ 28km (lidar) by Jäger (1992), and 17 ~ 25km (lidar) by Avdyushin et al. (1993).
 355 Based on comparison between simulated cloud with early infrared satellite images of Pinatubo,
 356 ? reported that the majority of ash was transported between 16km and 18km. This is
 357 physically understandable as particles are concentrated along intrusion height of umbrella
 358 cloud, not near top because the plume top is due to momentum overshoot. However, the
 359 empirical expressions for the height-MER relation, which are commonly adopted to cre-
 360 ate initial conditions for VATD simulation, tends to place majority of ash particles closer
 361 to top if use observed maximum height in the empirical expressions.



310 **Figure 7.** Comparison between “Semiempirical initial cloud + Puff” and “Plume-SPH +
 311 Puff”. Pictures from left to right are: Puff simulation based on initial condition created according
 312 to semiempirical plume shape expression, Puff simulation based on initial condition generated by
 313 Plume-SPH, TOMS or AVHRR image of Pinatubo ash cloud. Ash clouds at different hours after
 314 eruption are on different rows. From top to bottom, the images are corresponding to around 23
 315 hours after eruption (UT 199106160341), 31 hours after eruption (UT 199106161141), 55 hours
 316 after eruption (UT 199106171141). The observation data on the first row are TOMS ash and ice
 317 map. The observation data on the second and third row are AVHRR BTD ash cloud map with
 318 atmospheric correction method applied (?).

362 Here we check two commonly used plume shapes, the Poisson and Suzuki. For Pois-
 363 son plume shape, the vertical height of ash particles are determined according to Eq. (2).

$$H = H_{max} - 0.5H_{width} * P + H_{width}R \quad (2)$$

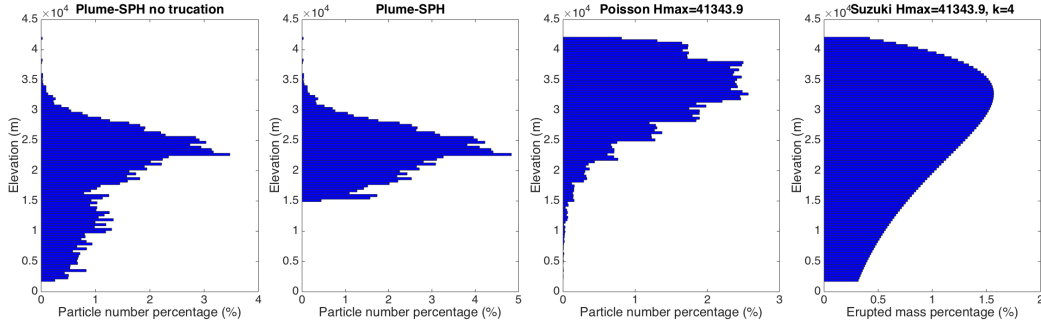
364 where P is an integral value drawn from a Poisson distribution of unit mean, R is a uni-
 365 formly distributed random number between 0 and 1, H_{max} is the maximum plume height,
 366 H_{width} represents an approximate vertical range over which the ash will be distributed.
 367 For Suzuki plume shape (T. Suzuki et al., 1983), volcano ash mass vertical distribution
 368 is assumed to follow the Suzuki equation (Eq. (3)).

$$Q(z) = Q_m * \frac{k^2(1 - z/H_{max})\exp(k(z/H_{max} - 1))}{H_{max}[1 - (1 + k)\exp(-k)]} \quad (3)$$

369 Where Q_m is the total mass of erupted material, k is shape factor, which is an adjustable
 370 constant that controls ash distribution with height. A low value of k gives a roughly uni-
 371 form distribution of mass with elevation, while high values of k concentrate mass near
 372 the plume top.

373 Particle distribution (in terms of mass percentage or particle number percentage)
 374 in vertical direction in the initial ash cloud are shown in Fig. 8. In that figure, the ver-
 375 tical particle distribution based on Plume-SPH output is compared with vertical par-
 376 ticle distribution created based on semieipirical shape expressions. Both Poisson and Suzuki

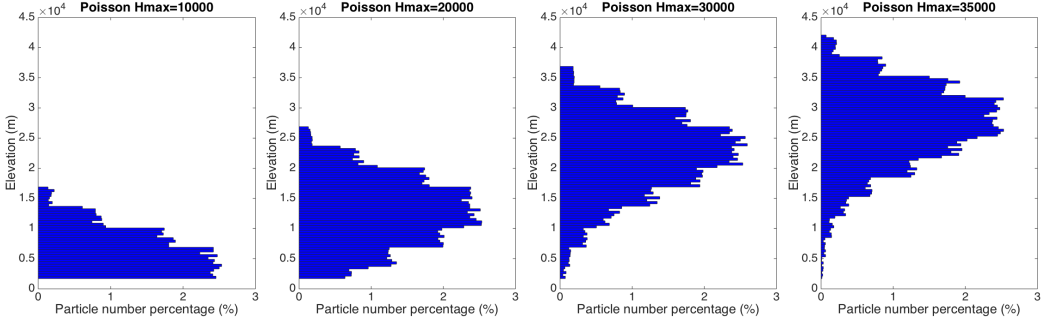
377 distribution in Fig. 8 take $H_{max} = 40000m$, which is close to reported observation of
 378 maximum height. When adopting Poisson plume shape, the majority of the particles are
 379 between $30km \sim 40km$. Obviously, Poisson distributes majority ash at a much higher
 380 elevation than observations (e.g. ?). As for Suzuki, the majority of ash particles also dis-
 381 tribute in a range that significantly higher than $25km$. As for initial ash cloud based on
 382 Plume-SPH simulation, the major population of ash particles distribute between $17km \sim$
 383 $28km$, which match well with observations. The maximum height is also consistent with
 384 observation. To summarize, using semiempirical plume shape expression generates un-
 385 realistic initial ash cloud even if we use observed plume maximum height.



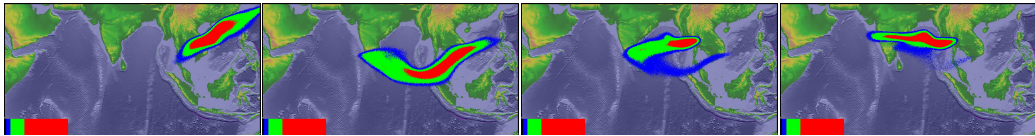
386 **Figure 8.** Particle distribution of initial ash cloud in vertical direction. The picture to the
 387 left is corresponding to initial ash cloud obtained from Plume-SPH output. The second picture
 388 is corresponding to ash distribution truncated by a elevation threshold of $15000m$. The third
 389 picture is for vertical ash distribution based on Poisson distribution with maximum height equals
 390 to $40000m$. Another parameter, the vertical spread, in the expression of Poisson plume shape is
 391 $6662m$. The picture to the right is corresponding to Suzuki distribution with maximum height
 392 equals to $40000m$. Another parameter in Suzuki distribution, the shape factor, is 4. The x axis is
 393 the percentage of particle number for Plume-SPH and Poisson. For Suzuki the x axis is the mass
 394 percentage of erupted material.

395 For Poisson and Suzuki plume shape, vertical distribution of ash particles can't be
 396 lower down without changing the maximum height. To distribute major population of
 397 ash particles at lower elevation, the maximum height has to be reduced to a value smaller
 398 than observed maximum height. Adjusting parameters such as maximum height in the
 399 emperical expression is actually the traditional source term calibration method. A set
 400 of initial ash clouds using different maximum heights based on Poisson plume shape is
 401 shown in Fig. 9). The maximum heights adopted in plume shape expressions are, by no
 402 means, obtained from any plume model or observation. Except for maximum height, all
 403 other parameters for creating initial ash cloud are the same as these in Table 4. The range,
 404 between which major populations of ash particles locate, is lower when using smaller max-
 405 imum heights. These ash clouds created by Poisson distribution with different maximum
 406 heights are then used as initial condition in Puff simulation, whose results are show in
 407 Fig. 10.

418 Figure 10 shows that the maximum height has significant influence on ash trans-
 419 portation simulation. When the maximum height is $10000m$ the high concentration area
 420 is lag behind observation. While the designated maximum height is $35000m$, the high
 421 concentration area is a little bit faster and much narrower than observation. When us-
 422 ing maximum height of $41343.9m$, the high concentration area is faster and narrower than
 423 both observation and “Pume-SPH+Puff” simulation results (see Fig. 7). The simulated
 424 high concentration area is closest to “Pume-SPH+Puff” simulation results when assign-
 425 ing a maximum height of $30000m$. The front of volcano ash, with lower concentration



408 **Figure 9.** Initial particle distribution in vertical direction based on Poisson plume shape with
 409 different maximum heights. Pictures from left to right are corresponding to maximum height of
 410 10000m, 20000m, 30000m, 35000m. Another parameter, the vertical spread, in the expression of
 411 Poisson plume shape is 6662m for all cases. The x axis is the percentage of particle number. See
 412 Fig. 8 for vertical ash distribution of Plume-SPH output.



413 **Figure 10.** Ash transportation simulated by Puff using different initial ash cloud created ac-
 414 cording to Poisson distribution with different maximum heights. Pictures from left to right are
 415 corresponding to maximum plume heights of 10000m, 20000m, 30000m and 35000m. All images
 416 are for simulated ash transportation around 55 hours after eruption (UT 199106171141). See the
 417 observed cloud image in Fig. 7.

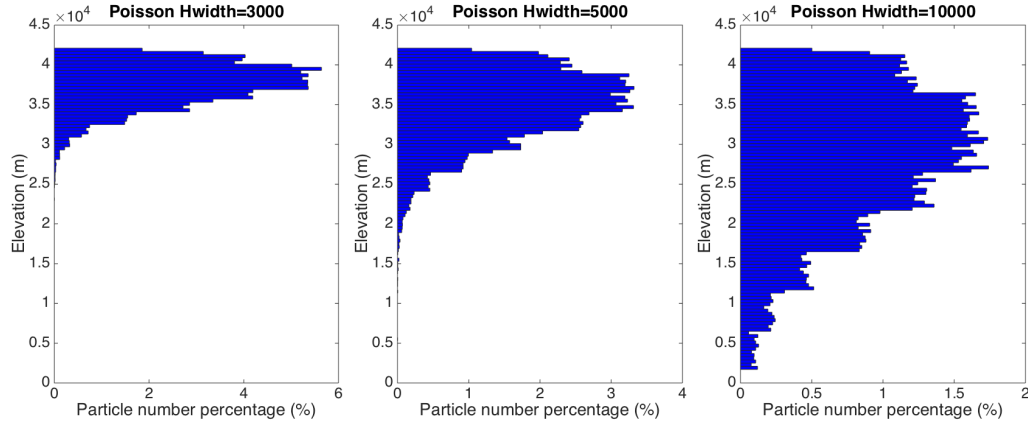
426 is faster than observation locating far west to high concentration area. A lower concen-
 427 tration tailing area also appears in the simulation results while there is no such tail in
 428 observed image. Puff simulation result based on calibrated maximum height of 30000m
 429 shows similar footprint to, even though smaller in terms of covered area than, those of
 430 "Pume-SPH+Puff" simulation. However, the initial ash cloud created by Poisson dis-
 431 tribution with maximum height around 20000m generates best match ash distribution
 432 with observation. That is to say, a maximum height lower than real maximum height
 433 is required by Poisson plume shape to distribute ash particles at the same elevation as
 434 real ash distribution. This is physically understandable as maximum plume heights are
 435 reached due to overshoot. Our hypothesis regarding the sources of disparity between "Semiem-
 436 pirical initial cloud +Puff" simulation and observation is confirmed. Since the initial con-
 437 dition has so dominant effect on VATD simulation, it is critical the forecast capability
 438 of VATD simulation to explore the more accurate and adaptive ways for establishing the
 439 initial conditions, especially the method that does not rely on "post event" parameter
 440 calibration.

441 3.3 Discussion Regarding Vertical Spread (H_{width})

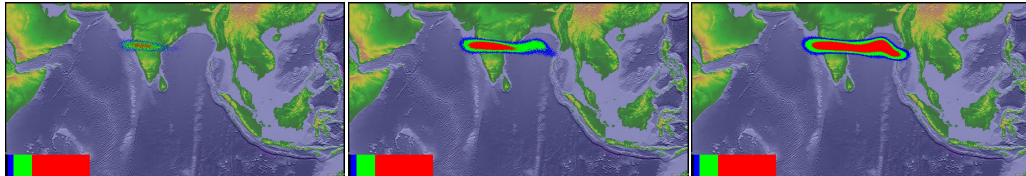
442 In previous section, the maximum height is adjusted to change vertical ash distri-
 443 bution along the source line. This section investigates another parameter in semiempir-
 444 ical possion expression. We vary the "vertical spread" (H_{width}) in range 3km/ 10km.
 445 A set of initial ash clouds created according to different "vertical spread" is shown in Fig.
 446 11. Except for "vertical spread", all other parameters for creating initial ash cloud are
 447 the same as these in Table 4. Width of the range within which major populations of ash
 448 particles locate become narrower when a smaller value for vertical spread is used. But

449 changing H_{width} has no obvious affect on the height at which majority of ash particles
 450 distribute. These ash clouds based on different vertical spread are then used as initial
 451 condition in Puff simulation, whose results are show in Fig. 12.

452 Adjusting of the vertical spread can change particle distribution in vertical direc-
 453 tion and not surprisingly affect VATD simulation results. Unluckily, none of these VATD
 454 simulations based on initial ash cloud with vertical spread equals to 3km, 5km, and 10km
 455 get better results than VATD simulation based on initial condition created by a 3D plume
 456 simulation using Plume-SPH (see Fig. 12).



457 **Figure 11.** Vertical particle distribution based on Poisson plume shape with different “ver-
 458 tical spread”. Pictures from left to right are corresponding to vertical spread of 3km, 5km and
 459 10km. The maximum height in the expression of Poisson plume shape is 40000m for all cases.
 460 The x axis is the percentage of particle number. See Fig. 8 for vertical ash distribution of Plume-
 461 SPH output.



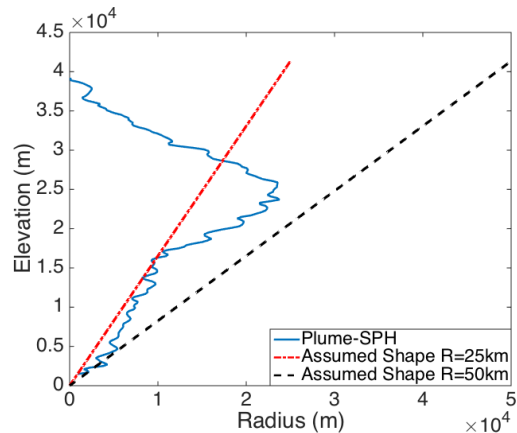
462 **Figure 12.** Ash transportation simulated by Puff using different initial ash cloud created with
 463 different vertical spread. Pictures from left to right are: Puff simulation results based on initial
 464 ash clouds with vertical spread equals to 3000mm, 5000mm and 10000m. The images are corre-
 465 sponding to around 55 hours after eruption (UT 199106171141). See the observed cloud image in
 466 Fig. 7. The simulated ash field does not adequately cover the observed ash field.

467 The calibrations carried out here are definitely not exhaustive. One might do more
 468 comprehensive calibration throughout the multi-dimensional parameter space (for Pois-
 469 son distribution, the parameter space is two dimension) and get better matched ash trans-
 470 portation results. With more complicated plume shape expression, one could have more
 471 control over plume shape and might be able to get initial condition that much closer to
 472 actual initial ash cloud, hence obtain more accurate ash transportation prediction. But
 473 more complicated plume shape expression usually leads to higher dimensional param-
 474 eter space which requires more effort to do calibration. Even though, the degree of free-
 475 dom to adjust plume shape is still limited. The new method for creating initial condi-

476 tions based on 3D plume simulation is more adaptive to various cases and obviates semiem-
477 pirical expressions regarding plume shape.

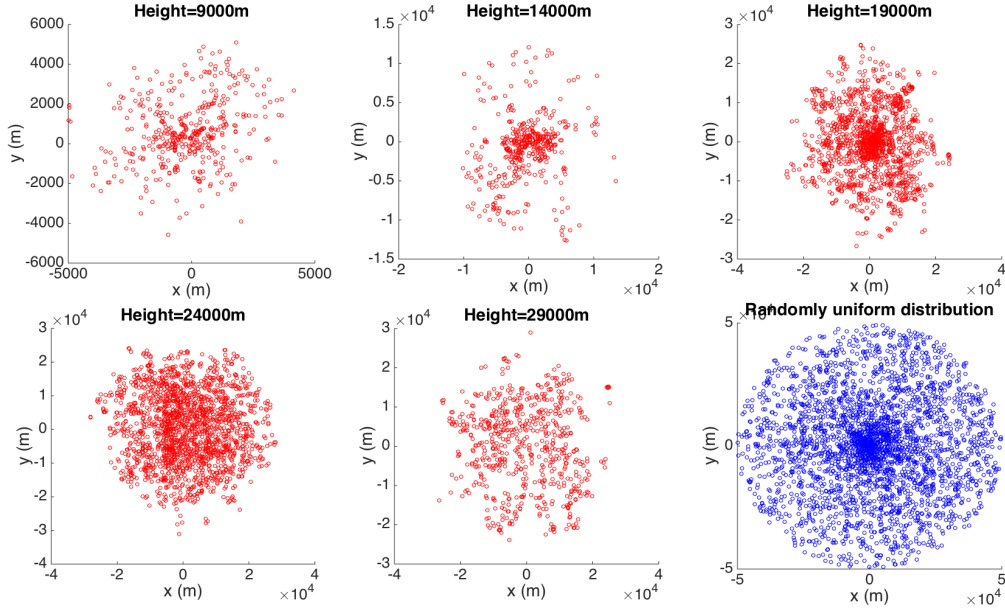
478 3.4 Horizontal Ash Distribution

479 The differences between assumed plume particle distribution and actual (or sim-
480 ulated by 3D plume) model are not only in vertical direction. How cloud horizontal par-
481 ticle distribution of the initial ash cloud affect ash transportation is investigated in this
482 section. Puff uses a uniformly distributed random process to determine the ash parti-
483 cle location in a circle centered on the volcano site. The maximum radius (at top) is given
484 as “horizontal spread” in Table 4. The horizontal displacement from a vertical line above
485 the volcano is a random value within a circle of radius, which equals to “horizontal spread”
486 multiplied by the ratio of the particle height H to maximum H_{max} . So the net shape
487 of the plume is an inverted cone where particles are located directly over the volcano at
488 the lowest level and extend out further horizontally with increasing plume height. As
489 for output of Plume-SPH, an effective radius is determined according to a given thresh-
490 old of ash concentration following Cerminara, Esposti Ongaro, & Neri (2016). A time
491 averaging and spatial integration of the dynamic 3D flow fields are conducted to get rid
492 of significant fluctuations in time and space. Fig. 13 compares radius of initial ash clouds
493 created by 3D plume simulation and assumed plume shape expression adopted in Puff.
494 Obviously, there is no chance for these two radius to be similar. Adjusting the param-
495 eter “horizontal spread” could not make the assumed plume shape to be similar to ash
496 cloud created by Plume-SPH. That is to say, merely parameter calibration is not enough
497 for such situation. It would require higher order semiempirical expression that takes more
498 parameters.



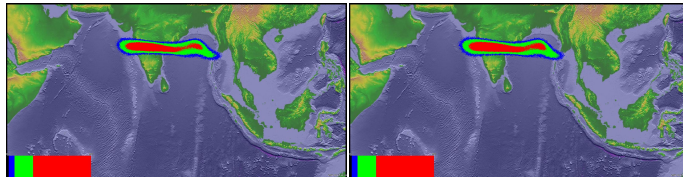
499 **Figure 13.** Comparison between radius of initial ash clouds created by 3D plume model
500 (Plume-SPH) and assumed initial ash cloud shape in Puff. The plume shape expression used in
501 Puff defines an inverted cone whose actual shape changes when “horizontal spread” takes differ-
502 ent values. $R = 25\text{km}$ is corresponding to “horizontal spread” equals to 50km . $R = 50\text{km}$ is
503 corresponding to “horizontal spread” equals to 100km

504 Comparison between cross-sectional views of the initial ash clouds is shown in Fig.
505 14. The cross-sectional view of assumed plume shape (last figure in Fig. 14) is similar
506 to cross-sectional view of simulated 3D plume in general sense. However, for simulated
507 3D plume, the ash particle distribution on cross section varies along with height. It is
508 hard for semiempirical expressions have such feature. In Puff, particle distribution on
509 cross sections is assumed to be the same.



510 **Figure 14.** Horizontal distribution of ash particles (tracers) on a cross section of initial ash
 511 cloud. Puff assumes randomly uniform distribution of ash particle within a circle, as shown by
 512 blue dots in the last figure. All other figures show ash particle distribution of initial ash cloud
 513 created by Plume-SPH at different elevations.

514 Assigning different values to “horizontal spread” has ignorable effect on VATD sim-
 515 ulation results. We use numbers between 50km to 1600km as “horizontal spread” to cre-
 516 ate initial ash cloud for VATD, all of them generate very similar results. Figure 15 shows
 517 two different simulation results based on initial ash cloud with “horizontal spread” equals
 518 to 50km and 600km respectively. No visible differences can be told between them. This
 519 implies that horizontal distribution has less significant influence on VATD simulation re-
 520 sults than vertical distribution.



521 **Figure 15.** Ash transportation simulated by Puff at around 55 hours after eruption (UT
 522 199106171141). Different values for “horizontal spread” are used to create initial ash cloud. Pic-
 523 tures to the left is corresponding to “horizontal spread” equals to 50kmm . Pictures to the right is
 524 corresponding to “horizontal spread” equals to 600kmm . The observed cloud image is in Fig. 7.

525 4 Conclusion

526 This paper presented, for the first time, VATD simulations using intial conditions
 527 created by a 3D plume model. Traditional VATD simulations use initial conditions cre-
 528 ated according to a semiempirical plume shape expression. A case study of the 1991 Pinatubo
 529 eruption demonstrates that a 3D plume model can create more realistic initial ash cloud

530 and ash parcel positions, and therefore improve the accuracy of ash transport forecasts.
 531 Informal sensitivity analyses suggest that initial conditions, as expressed in the dispo-
 532 sition of initial ash parcel positions in the vertical, have a more significant effect on a vol-
 533 canic ash transport forecast than most other parameters. Comparison of initial ash par-
 534 cel distributions among the 3D plume model, semiempirical expressions, and observa-
 535 tions suggests that a major subpopulation of ash parcels should be placed at a much lower
 536 elevation than maximum height to obtain a better VATD forecast. For the Pinatubo case
 537 study, “well-matched” simulation results are observed when using a maximum height of
 538 around 30km, which is much lower than the observed maximum height of 40km. Com-
 539 paring the effects of the maximum height, vertical spread and horizontal spread shows
 540 that ash particle distribution in the vertical direction has the strongest effect on VATD
 541 simulation.

542 We have presented a novel method for creating *a priori* initial conditions for VATD
 543 simulations. We have shown that it might be possible to obtain initial positions of ash
 544 parcels with deterministic forward modeling of the volcanic plume, obviating the need
 545 to attempt to obtain initial positions or a history of release heights via inversion (Stohl
 546 et al., 2011). Although the method now suffers from the high computational cost asso-
 547 ciated with 3D forward modeling, it not only helps overcome shortcomings of existing
 548 methods used to generate *a priori* input parameters, but also overcomes the need to do
 549 the thousands of runs associated with inverse modeling. In addition, computational cost
 550 will continue to diminish as computing speed increases. As they are forward numerical
 551 models based on first principles, 3D plume models need little if any parameterization,
 552 and user intervention should not be required to improve forecast power; no assumption
 553 about the initial position of ash parcels is needed. Generation of the initial cloud of ash
 554 parcels directly by 3D simulation is potentially adaptable to a variety of volcanic and
 555 atmospheric scenarios. In contrast, semiempirical expressions used to determine initial
 556 conditions require several parameters to control ash particle distribution along a verti-
 557 cal line source or some simplified shape of the initial ash cloud, making it difficult in some
 558 cases to generate initial conditions that closely resemble a complex reality.

559 The full range of research issues raised by numerical forecasting of volcanic clouds
 560 is diverse. We described in this paper the effect of initial conditions chosen from the out-
 561 put of a 3D plume model on numerical forecasts of volcanic ash transport simulation.
 562 The wind field, another important factor in volcanic ash transportation simulation is not
 563 discussed in the present work. Some other aspects, such as small scale physical processes,
 564 even though they play lesser roles, might need to be included in VATDs to improve ac-
 565 curacy for a particular eruption. In addition, eruption conditions are subject to change
 566 with time, even during the climactic phase of an eruption. In the future, time-dependent
 567 initial conditions for VATDs can be created from 3D plume simulations with time-dependent
 568 eruption conditions.

569 Acknowledgments

570 Support for the Twentieth Century Reanalysis Project dataset is provided by the U.S.
 571 Department of Energy, Office of Science Innovative and Novel Computational Impact
 572 on Theory and Experiment (DOE INCITE) program, and Office of Biological and En-
 573 vironmental Research (BER), and by the National Oceanic and Atmospheric Adminis-
 574 tration Climate Program Office.

575 References

- 576 (n.d.).
 577 Avdyushin, S., Tulinov, G., Ivanov, M., Kuzmenko, B., Mezhuev, I., Nardi, B., ...
 578 Chanin, M.-L. (1993). 1. spatial and temporal evolution of the optical thick-
 579 ness of the pinatubo aerosol cloud in the northern hemisphere from a network of

- 580 ship-borne and stationary lidars. *Geophysical research letters*, 20(18), 1963–1966.
- 581 Bonadonna, C., & Houghton, B. (2005). Total grain-size distribution and volume of
582 tephra-fall deposits. *Bulletin of Volcanology*, 67(5), 441–456.
- 583 Bursik, M. (2001). Effect of wind on the rise height of volcanic plumes. *Geophys.
584 Res. Lett.*, 28(18), 3621–3624.
- 585 Cao, Z., Patra, A., Bursik, M., Pitman, E. B., & Jones, M. (2018). Plume-sph 1.0:
586 a three-dimensional, dusty-gas volcanic plume model based on smoothed particle
587 hydrodynamics. *Geoscientific Model Development*, 11(7), 2691–2715.
- 588 Cerminara, M., Esposti Ongaro, T., & Berselli, L. (2016). Ashee-1.0: a compressible,
589 equilibrium-eulerian model for volcanic ash plumes. *Geoscientific Model Develop-
590 ment*, 9(2), 697–730.
- 591 Cerminara, M., Esposti Ongaro, T., & Neri, A. (2016). Large eddy simulation of
592 gas-particle kinematic decoupling and turbulent entrainment in volcanic plumes.
593 *Journal of Volcanology and Geothermal Research*.
- 594 Costa, A., Suzuki, Y., Cerminara, M., Devenish, B., Esposti Ongaro, T., Herzog, M.,
595 ... others (2016). Results of the eruptive column model inter-comparison study.
596 *Journal of Volcanology and Geothermal Research*.
- 597 Daniele, P., Lirer, L., Petrosino, P., Spinelli, N., & Peterson, R. (2009). Applications
598 of the puff model to forecasts of volcanic clouds dispersal from etna and vesuvio.
599 *Computers & Geosciences*, 35(5), 1035–1049.
- 600 de'Michieli Vitturi, M., Neri, A., & Barsotti, S. (2015). Plume-mom 1.0: A new
601 integral model of volcanic plumes based on the method of moments. *Geoscientific
602 Model Development*, 8(8), 2447–2463.
- 603 Draxler, R. R., & Hess, G. (1998). An overview of the hysplit_4 modelling system for
604 trajectories. *Australian meteorological magazine*, 47(4), 295–308.
- 605 Damours, R. (1998). Modeling the etex plume dispersion with the canadian emer-
606 gency response model. *Atmospheric Environment*, 32(24), 4335–4341.
- 607 Folch, A., Costa, A., & Macedonio, G. (2009). Fall3d: A computational model for
608 transport and deposition of volcanic ash. *Computers & Geosciences*, 35(6), 1334–
609 1342.
- 610 Folch, A., Costa, A., & Macedonio, G. (2016). Fplume-1.0: An integral volcanic
611 plume model accounting for ash aggregation. *Geoscientific Model Development*,
612 9(1), 431.
- 613 Jäger, H. (1992). The pinatubo eruption cloud observed by lidar at garmisch-
614 partenkirchen. *Geophysical research letters*, 19(2), 191–194.
- 615 Mastin, L. G. (2007). A user-friendly one-dimensional model for wet volcanic
616 plumes. *Geochemistry, Geophysics, Geosystems*, 8(3).
- 617 Neri, A., Esposti Ongaro, T., Macedonio, G., & Gidaspow, D. (2003). Multiparti-
618 cle simulation of collapsing volcanic columns and pyroclastic flow. *Journal of Geo-
619 physical Research: Solid Earth (1978–2012)*, 108(B4).
- 620 Oberhuber, J. M., Herzog, M., Graf, H.-F., & Schwanke, K. (1998). Volcanic plume
621 simulation on large scales. *Journal of Volcanology and Geothermal Research*,
622 87(1), 29–53.
- 623 Pouget, S., Bursik, M., Singla, P., & Singh, T. (2016). Sensitivity analysis of a one-
624 dimensional model of a volcanic plume with particle fallout and collapse behavior.
625 *Journal of Volcanology and Geothermal Research*.
- 626 Schwaiger, H. F., Denlinger, R. P., & Mastin, L. G. (2012). Ash3d: A finite-volume,
627 conservative numerical model for ash transport and tephra deposition. *Journal of
628 Geophysical Research: Solid Earth*, 117(B4).
- 629 Searcy, C., Dean, K., & Stringer, W. (1998). Puff: A volcanic ash tracking and pre-
630 diction model. *Journal of Volcanology and Geothermal Research*, 80, 1–16.
- 631 Stohl, A., Prata, A., Eckhardt, S., Clarisse, L., Durant, A., Henne, S., ... others
632 (2011). Determination of time-and height-resolved volcanic ash emissions and
633 their use for quantitative ash dispersion modeling: the 2010 eyjafjallajökull erup-

- 634 tion. *Atmospheric Chemistry and Physics*, 11, 4333–4351.
- 635 Suzuki, T., et al. (1983). A theoretical model for dispersion of tephra. *Arc volcan-*
636 *ism: physics and tectonics*, 95, 113.
- 637 Suzuki, Y., & Koyaguchi, T. (2009). A three-dimensional numerical simulation of
638 spreading umbrella clouds. *Journal of Geophysical Research: Solid Earth* (1978–
639 2012), 114(B3).
- 640 Suzuki, Y. J., Koyaguchi, T., Ogawa, M., & Hachisu, I. (2005). A numerical study
641 of turbulent mixing in eruption clouds using a three-dimensional fluid dynamics
642 model. *Journal of Geophysical Research: Solid Earth*, 110(B8).
- 643 Tanaka, H. (1991). Development of a prediction scheme for the volcanic ash fall
644 from redoubt volcano. In *First int'l. symp. on volcanic ash and aviation safety*
645 (Vol. 58).
- 646 Tupper, A., Itikarai, I., Richards, M., Prata, F., Carn, S., & Rosenfeld, D. (2007).
647 Facing the challenges of the international airways volcano watch: the 2004/05
648 eruptions of manam, papua new guinea. *Weather and Forecasting*, 22(1), 175–
649 191.
- 650 Walko, R., Tremback, C., & Bell, M. (1995). Hypact: The hybrid particle and con-
651 centration transport model. *Users guide*.
- 652 Witham, C., Hort, M., Potts, R., Servranckx, R., Husson, P., & Bonnardot, F.
653 (2007). Comparison of vaac atmospheric dispersion models using the 1 november
654 2004 grimsvötn eruption. *Meteorological Applications*, 14(1), 27–38.
- 655 Woods, A. (1988). The fluid dynamics and thermodynamics of eruption columns.
656 *Bulletin of Volcanology*, 50(3), 169–193.
- 657 Zidikheri, M. J., Lucas, C., & Potts, R. J. (2017). Estimation of optimal dispersion
658 model source parameters using satellite detections of volcanic ash. *Journal of Geo-
659 physical Research: Atmospheres*, 122(15), 8207–8232.